Development of an innovative double-swept rotor blade tip for the rotor test facility Goettingen

M.M.Mueller, T.Schwermer, H.Mai and C.Stieg

Abstract—Innovative double-swept rotor blade tip planforms show significant potential to reduce noise and vibrations while improving the overall performance. Current test results for a non-rotating double-swept innovative rotor blade tip model, inspired by the DLR patent "Erato", were obtained in a conventional wind tunnel (DNW TWG, Transonic Wind Tunnel Goettingen) under forced pitching motions. In the next step, the influence of rotation and the environment of an entire rotor head system should be considered. It is of great interest to investigate the influence of rotation on the aeroelastic behaviour and the unsteady aerodynamics in a dedicated further experiment. The Rotor Test Facility Goettingen (RTG) was built for research on rotating rotor blades under optimized boundary conditions and will be used for the planned experiments. Typical flow phenomena associated with rotor blades will be investigated, such dynamic stall, compression shocks as well as aeroelastic stability. For that purpose new innovative double-swept rotor blades for the RTG have been developed at the DLR Institute of Aeroelasticity in Goettingen. The design of the planform is partially based on the existing wind tunnel model. Further profile sections and a rotor head attachment were added. Design load cases were determined from two dimensional numerical flow simulations regarding several rotor blade sections. A finite element analysis, including fatigue analysis, was carried out as well. In order to extract the dominant flow phenomena the rotor blades are instrumented with unsteady pressure transducers, temperature transmitters and strain gauges. The acquired data will enable subsequent evaluation concerning aeroelastic stability of the entire rotor head system and the rotor blade tip geometry. Furthermore the influence of rotation on the dynamic stall phenomenon can be assessed.

NOTATION

CFRP	Carbon fiber reinforced plastic
DNW	German Dutch wind tunnels
TWG	Transonic wind tunnel Goettingen
RTG	Rotor test facility Goettingen
DLR	German aerospace center
GVT	Ground vibration test
MDR	Magnetic dependent resistor
CFD	Computational fluid dynamics
FEM	Finite element method

1 INTRODUCTION

In manufacturing of helicopter rotor blades double-swept planforms come more and more into focus, because these planforms show huge potential to reduce noise and enhance the overall performance. However, the aeroelastic stability as well as the dynamic stall behaviour of a double-swept rotor blade is a challenge, because aeroelastic stability as well as dynamic stall limit the flight envelope of helicopters. Therefore, the investigation of the named effects on double-swept rotor blades is of great interest.

Helicopter rotor blades do a cyclic pitching motion to balance the moments and forces around the rotation axes and to control the helicopter. Dynamic stall occurs on the retreating rotor blades in forward and maneuvering flight conditions. The aeroelastic stability of the rotor head depends on the eigenfrequencies and eigenvalue of the rotor blade and the aeroelastic behaviour of the rotor head. On the retreating blade, where dynamic stall is located are low local flow conditions and high angels of attack. During dynamic stall high increasing lift and strong negative pitching moment occur. That leads to vibration, high rotor blade and pitching link loads, which influence the aeroelastic stability. Furthermore there are compression shocks, dynamic blade loads and blade vortex interactions at the rotor head system. Every single of these effects differs in onset and behaviour in comparison to a conventional rotor blade tip planform. Of great interest is the influence of the type and strength of these effects by the planform.

With a better understanding of the dynamic stall phenomenon and aeroelastic behaviour of double-swept rotor blades future innovative rotor blade designs could be improved. Safe operation of innovative rotor blades can be ensured and aerodynamic and aeroelastic computation can be validated. Furthermore understanding the influence of the forward and backward swept part on dynamic stall, aeroelastic behaviour and total blade deformation is advantageous for future rotor blade tip modeling.

Helicopter rotor blades are highly influenced by three-

- *M.M. Mueller is with the Institute of Aeroelasticity, German Aerospace Center (DLR), 37073 Göttingen, m-mmueller@dlr.de.*
- *T. Schwermer is with the Institute of Aerodynamics, German Aerospace Center (DLR), 37073 Göttingen, Till.Schwermer@dlr.de.*
- *H. Mai is with the Institute of Aeroelasticity, German Aerospace Center (DLR), 37073 Göttingen, Holger.Mai@dlr.de.*
- *C.Stieg is with the Institute of Aeroelasticity, German Aerospace Center (DLR), 37073 Göttingen, Christian.Stieg@dlr.de.*

dimensional effects, like radial acceleration of flow components and increasing Mach number along the blade. To consider all these effects the rotor test facility Goettingen (RTG) will be used for the planed experiments. A new innovative double-swept rotor blade tip model was developed in the Institut of Aeroelasticity in Goettingen. The model will be equipped with several measurement techniques, like pressure transducers, strain gauges and temperature sensors. In addition, the non-contact measurement techniques Particle Image Velocimetry (PIV) and Stereo Pattern Recognition (SPR) can be used.

2 Wind tunnel model

The innovative double-swept rotor blade tip for the RTG is based on an already existing double-swept rotor blade tip wind tunnel model, for the Transonic Wind Tunnel Goettingen (DNW-TWG). This was developed as a part of a DLR project [5]. The planform geometry of the rotor blade tip wind tunnel is inspired by the ERATO geometry [10], [11]. The wind tunnel model was built with Carbon Fiber Reinforced Plastic (CFRP) because of the space for instrumentation, stability requirements and weight. The model consists of a lower shell, upper shell and a double C-spar with foam core. For the connection to the hydraulic oscillation rig the wind tunnel model has a steel shaft embedded in the upper and lower composite shell. The model was developed for 3D dynamic stall investigations in the DNW-TWG with an oscillation test rig, which set the model to a pitching motion. The cross section of the DNW-TWG is $1x1m^2$ and has a flexible top and bottom wall in the adaptive test section. The wind tunnel has a Mach number range from $Ma = 0.3-0.9$. Furthermore the wind tunnel can be pressurized from $0.3 < p_0 < 1.5$ bar. Thereby Reynolds numbers of $Re = 1.2 * 10^6$ can be achieved with a root chord length of $c = 160$ mm [7], [6].

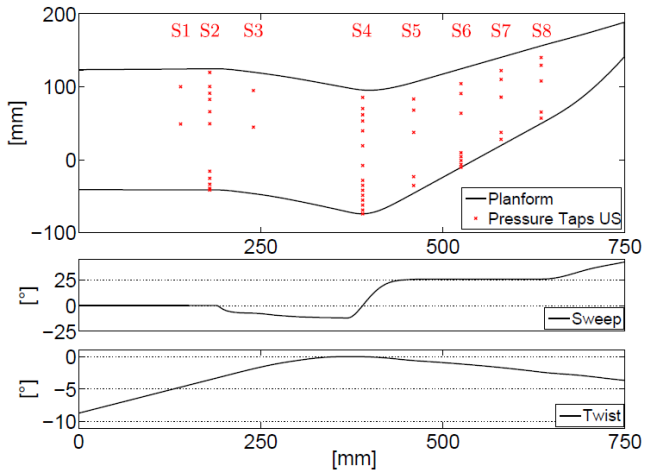

Fig. 1. Twist and sweep of the double-swept rotor blade tip wind tunnel model [6]

The double-swept rotor blade tip wind tunnel model has a span width of $s = 750mm$ in order to minimize the interaction of the blade tip vortex with the wind tunnel wall. The chosen chord length varies from the root (c_{root}= $166.5mm$) to the blade tip (c_{tip} = $45mm$) (see figure 1). The resultant aspect ratio of the wind tunnel model is AR = 4.5. The forward sweep of $\Lambda = 11°$ begins at $r = 200mm$ and ends at $r = 390mm$. A maximum backward sweep of Λ = $25.7°$ goes up to r = $638mm$. The sweep area reduces the effective Mach number and thus also the compressibility effects. The airfoils that have been used for this model are the $EDI - M112$ and the $EDI - M109$ [5], [6], [7]. From the root up to the beginning of the forward sweep the $EDI - M112$ airfoil is used. In the backward swept part the $EDI - M109$ airfoil is used. Between the airfoils $EDI - M109$ and $EDI - M112$ a transitional area of aerodynamic restriction is obtained. The spanwise twist trend goes from $-8,7°$ at the root up to $0°$ on the kink. From the beginning of the backward swept part up to the blade tip the twist decreases from $0°$ to $-3.5°$ [5]. The high negative twist angle at the root was used to avoid early flow stall at the root caused by the wind tunnel boundary layer at high angles of attack. In context of the development a detailed CAD model as well as a high fidelity 3D finite element model were generated.
The model is equipped with 58 unsteady pressure transducers distributed on eight spanwise sections (see figure 1). Furthermore two unidirectional acceleration sensors (flap and lead-lag direction) and two temperature sensors (upper and lower composite shell) are integrated. Additional measurement techniques, where used in the experiments. A Magnetic Dependent Resistor (MDR) was mounted on the hydraulic cylinder to measure the angle of attack. Another technique to measure the angle of attack are two fixed triangulation-based laser, which measure the distance to a beam. This beam is mounted between the hydraulic cylinder and the models root outside the wind tunnel. A marker based photogrammetry system is used to measure the total deformation. Two high speed cameras outside of the wind tunnel are used to track thin surface marker continuously. With a piezoelectric balance the global internal forces (lift, drag, pitching moment) are measured. The balance was mounted outside the wind tunnel between the beam for measuring the angle of attack and the hydraulic cylinder. In every experiment a infrared camera is used to detect transition or compression shocks on the surface. In the second experiment, where the focus was on the investigation of dynamic stall, pressure sensitive paint was used to visualize stall areas. In addition, a Ground Vibration Test (GVT) was carried out prior to the experiments to identify the eigenformen and eigenfrequencies [5], [6].

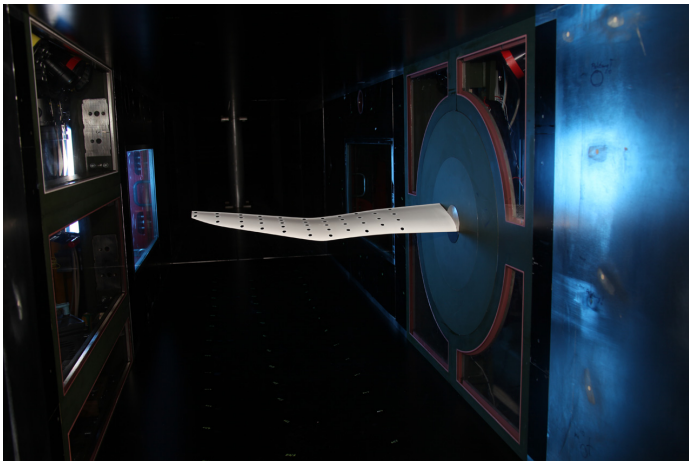

Fig. 2. Rotor bade tip wind tunnel model [6]

In the framework of a DLR project three wind tunnel tests were conducted (figure 2). The wind tunnel tests have given first indentations about the flow conditions, aeroelastic behaviour and influence of the double-swept part [5]. The first wind tunnel experiment was carried out to test the model. In the second experiment, a retreating rotor blade tip was modeled, where the focus was on the investigation of dynamic stall. In the third experiment the aerodynamic and aeroelastic behaviour of a advanced rotor blade tip was investigated. One of the essential findings of the first two experiments is that the time shifted stall behaviour of the forward and backward swept part lead to a reduction of the pitching moment derivative. The data of the third experiment is still been analyzed. For more information about the experiments and result look at [5], [6]. However all wind tunnel experiments did not consider the three-dimensional effects that helicopter rotor blades are exposed to. Therefore, a RTG model was derived from the wind tunnel model.

3 Rotor Test Facility Goettingen (RTG)

The Rotor Test Facility Goettingen was developed by the Institute of Aerodynamics and Flow Technology [1] in Goettingen. The facility was designed for dynamic stall investigations of a two or four bladed rotor. It is a Mach scaled rotor. So investigations can be done at realistic reduced frequencies.

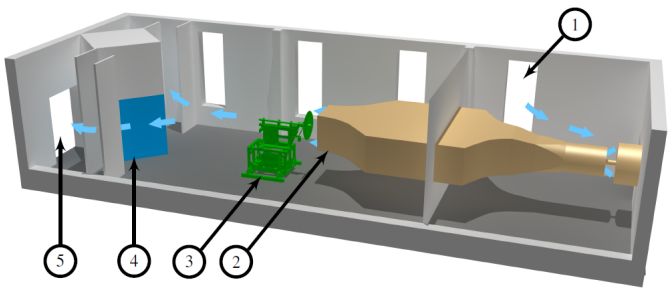

Fig. 3. Overview rotor test facility Goettingen [1]

Figure 4 shows an overview of the Rotor Test Facility Goettingen. The test facility consists of a rotor test bench (4), Eiffel type wind tunnel (2), control room (4) and several air outlet (5) and inlet (1) possibilities at the building. The air inlet and outlet are in separate rooms to avoid recirculation in the test facility. The rotor test bench is mounted vertically in front of an existing Eiffel type wind tunnel. The wind tunnel blows the air onto azimuth level of the rotor. So the Eiffel type wind tunnel provides a defined inflow. The rotor vortex system can be convected downstream to avoid blade vortex interactions. The nozzle of the Eiffel wind tunnel has a rectangular cross section ($1.6x3.2$ m^2) and a maximum freestream Mach number of $Ma = 0.04$. Because of the cross section size, the maximum rotor radius is limited to $R = 0.65$ m. With the radius and a rotational frequency of $f_{rot} = 50Hz$ a realistic tip Mach numbers of $Ma = 0.6$ can be achieved. After the rotor test bench the airflow passes the control room on both sides through a labyrinth outwards [1].
As can be seen in figure 4 the rotor test bench consists of an electric motor, a drive shaft with cardan joint (beared on four points), a rotor head system, a piezoelectric balance mounted under the first two bearings and an actuator with shaft for turning around the swashplate. At the end of the main shaft a rotary encoder is mounted to determine the rpm. The main rotor shaft and electric motor are linked with a toothed belt.

The rotor head of the RTG has a compact design and must comply several conditions. First, the maximum possible rotor radius is $R = 0.65m$, therefore it is necessary to start with the aerodynamic shape as close to the rotor head as possible. The aerodynamic shape starts at $(r/R = 0.25)$. Furthermore rotational frequencies of $f_{rot_{max}} = 65Hz$ lead to high centrifugal forces and high static aerodynamic forces. This results in specific strength requirements on the rotor head, rotor blades and equipped instrumentation. The rotor head system consists of the main hub, four or two mounted blades, fully functional swashplate, Datatel 30 channel telemetry system ($19kHz$ bandwidth per channel) and a universal-mounted rotor blade connection. The swashplate is used to set the angle of attack in collective, cyclic or a combination. Of both, cyclic and collective angle can be adjust independent from each other. The step actuator, shaft and worm gear are special for this test facility. They are used to rotate the swashplate stationary with a second static swashplate. The second swashplate is connected with the worm gear and the right swashplate. So it is possible to rotate every azimuth position of a pitch cycle to one measurement position. In the universal-mounted rotor blade connection are two radial ball bearings to support the pitch links and one axial ball bearing to transfer the centrifugal forces. A hall sensor is used to measure the angle of attack in the rotor head. For more information of the rotor head design see [1]. Dynamic stall at the RTG is preferred induced with the swashpalte. A high collective and cyclic angle of attack

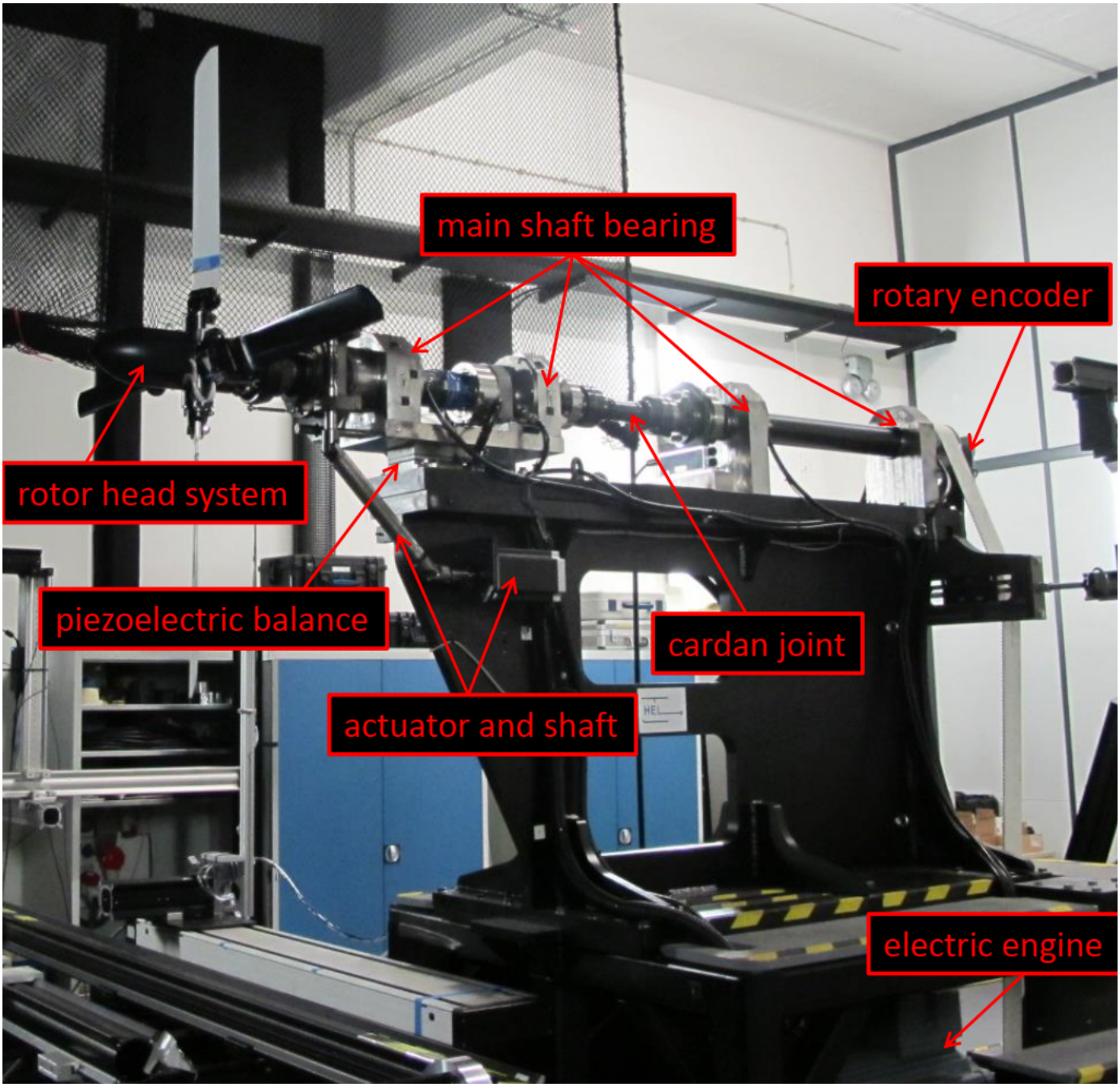

Fig. 4. Rotor test bench

were adjusted to simulate a retreating rotor blade and triggered the dynamic stall phenomenon. Dynamic stall and wake vortex experiments with a straight rotor blade set were done and generated interesting results [2], [4], [9]. In Addition to the experiments three dimensional CFD computations were done [3], [8].

4 Rotor blade

In further experiments the 3D effects of a rotor blade should be taken into account. Therefore an innovative double-swept rotor blade is derived from the wind tunnel model described above. The rotor blade has to be constructed structural by as rigid as possible due to its small size. This condition leads to the following design chain: The first step is to generate a full CAD model with exact positions of the instrumentation. The second step is the load prediction, based on the CAD model. The last step is the structural design and instrumentation. The structural design is adjusted to the predicted load, because high loads occur on the blades. The instrumented rotor blades are previously designed for the investigation of dynamic stall and aeroelastic stability.

4.1 CAD design and instrumentation

The CAD design became more difficult than previously thought because of the innovative planform. At the CAD design two boundary conditions have to be considered. First the maximum rotor radius dosen't have to be exceeded. Second the chord length is limited at $72mm$. The rotor blade is designed with a combination of the $EDI - M109$ and $EDI - M112$ airfoil geometries. The maximum chord length is $c = 72mm$ at the root. The chord length achieve its minimum with $c = 72mm$ on the blade tip. In addition to the radial tapering there are a forward and backward sweep of the leading and trailing edge. The leading, upper and lower trailing edge as well as the airfoil geometries $EDI - M109$ and $EDI - M112$ are generated with dot clouds. With the dot clouds airfoil and leading splines are created. The basic geometry is generated in original rotor blade size. For the construction of the surface model a combination of eleven spanwise $EDI - M109$ and $EDI - M112$ airfoil geometries are used. Eight of these spanwise sections shift forward and backward in chordwise direction to generate the sweep. The same forward and backward shift is done with the leading and trailing edge as can be seen in figure 5.

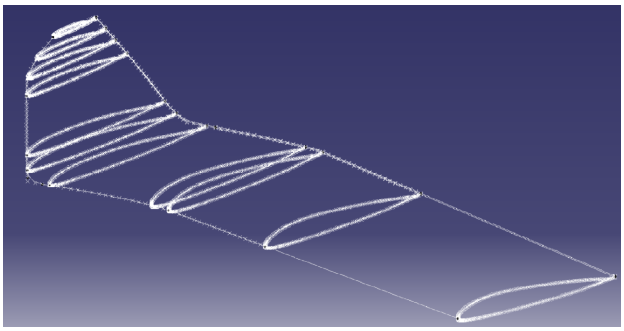

Fig. 5. Airfoil, leading and trailing edge splines

The shifting chordwise distance, twist and tapering of the used spanwise airfoils are defined previously. The coordinates of the dot clouds are adjusted via geometric relations to reach the desired spanwise twist, tapering and sweep. As mentioned in chapter 2 the planform of the innovative double-swept rotor blade is based on the existing double-swept wind tunnel model. However, with just the down scaled wind tunnel geometry the desired rotor radius of $R = 0.65m$ can not be achieved. Therefore, the geometrie is extended by the corresponding length of the $EDI - M112$ airfoil. The extension of the geometry is done in original rotor blade size. After the extension a surface model was created and scaled down to the desired chord length. The strong down sizing of the geometry led to bad spanwise transitions between the airfoil and airfoil shapes with bad curvature. To correct the transition areas and airfoil shapes the splines are modified. To correct the shapes some dots in the airfoil, leading and trailing edge were deleted to get a smooth curvature trend for every airfoil. In order to obtain smooth transitions on the leading and trailing edge, the tangential conditions were adjusted. For manufacturing reasons the trailing edge has to be thickened to $0,5mm$. After the adjustments and down-sizing a smooth and closed surface of the innovative double-swept rotor blade is obtained, as seen in figure 6. From the surface model a full model is generated. The rotor blade geometry is extended with a model foot, in order to have a connection with the rotor head. The parallel upper and lower side of the model foot is the reference surfaces for the measurement of the angle of attack. The chord at the root has a negative twist of $-1.3°$ to the reference surfaces. The rotor blade is mounted to the rotor head with two connecting bolts .

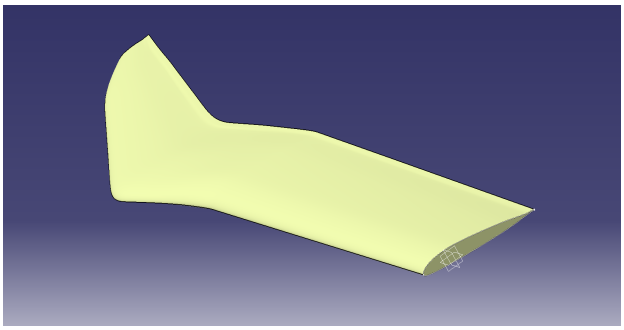

Fig. 6. Shape model of the innovative double-swept rotor blade

Despite the small dimensions of the rotor blade, 22 unsteady pressure transducers (Kulite LQ-062) can be integrated underneath the surface. The pressure transducers are the sealed gage version. They measure the surface pressure distribution. The 22 Kulites are divided over 7 spanwise sections. There are two high instrumented sections at $r/R = 0.52$ and $r/R = 0.71$ to detect the flow phenomena. A third section is on the backward swept part which has less Kulites at $r/R = 0.83$. Due to the thickness and small chord length of the airfoil at this position it is not possible to integrate more pressure transducers. As seen in figure 7 the place for pressure transducers (1.6 x 4.7 x 0.8 mm) is limited by the thickness of the sections as well as in outer spanwise sections by the chord length. Every sensor reduces the mechanical strength of the structure due to milled pockets for the sensors and their cables. So, the total amount of sensors is limited. As figure 7 shows in cut A-A there is a small pocket for a mounting tube, which connects the sensor with the shell. Every sensor and tube is oriented normal to the blade surface. This mounting technique was also used at the first rotor blades for the RTG [1]. It should obtain low damping of the pressure signal that ensure natural frequency above the bandwidth of the telemetry system. In addition to the pressure transducer, there are two Pt100 temperature sensors at $r/R = 0.66$ underneath the rotor blade surface. The temperature of resin has to be monitored during the measurement, because it can rise up to critical temperatures.

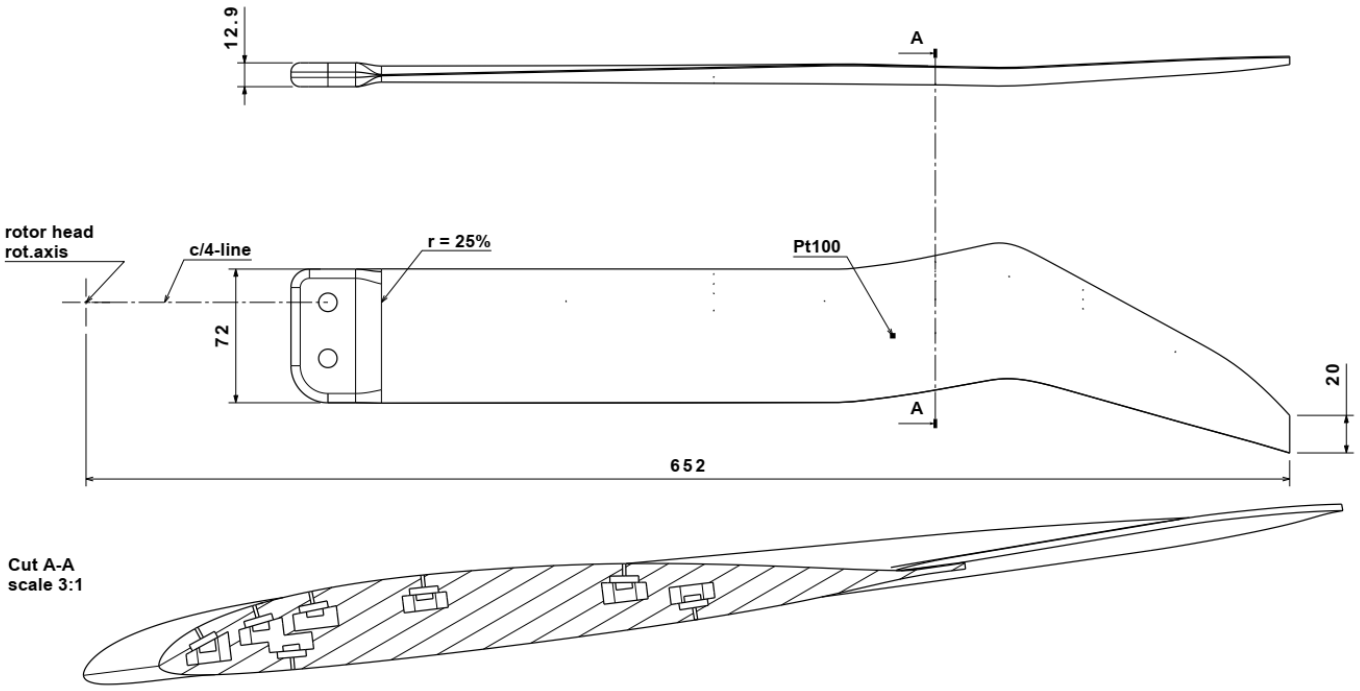

Fig. 7. Final geometry of the innovative double-swept rotor blade and pressure transducer distribution in a high instrumented section

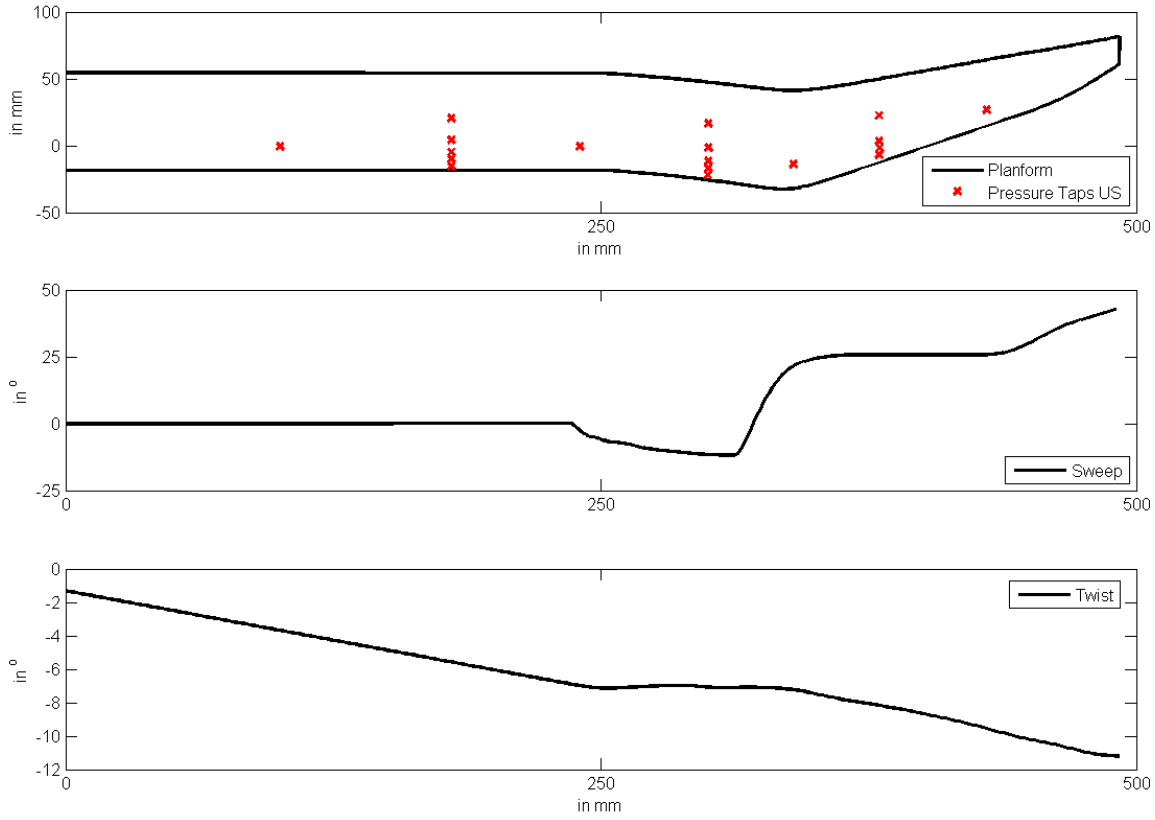

Fig. 8. Spanwise twist and sweep distribution and distribution of all pressure transducers

Figure 7 and 8 depict the final planform and pressure transducer distribution of the upper shell as well as the spanwise twist and sweep. The spanwise sweep at the forward and backward swept part is equal to the existing wind tunnel model. A maximum forward sweep of $\Lambda = 11°$ until $r/R = 0.76$ and maximum backward sweep of $\Lambda = 25.7°$ until $r/R = 0.95$ can be seen. The spanwise twist distribution is changed in comparison to the wind tunnel model. A negative twist is used around the quarter chord line. The twist begins at the root ($r/R = 0.25$) with $\alpha = -1.2°$ and drops to $\alpha = -7°$ at $r/R = 0.63$. After that starts a constant part at the forward sweep with $\alpha = -7°$ until $r/R = 0.77$. From the kink the twist decreases from $\alpha = -7°$ until $\alpha = -10.5°$ on the blade tip. The appropriation of the airfoils is as follows, from the root until the beginning of the forward swept part the $EDI - M112$ is used. The $EDI - M109$ is used from the beginning of the backward swept part.

4.2 Load prediction

The prediction of the aerodynamic design loads were carried out with unsteady Computational Fluid Dynamics (CFD). The approach was the same as for the first rotor test facility blades [1]. Due to more complex planform of the innovative rotor blade the calculation was more difficult and needed a few adjustments. As with the last rotor blade set an unsteady three-dimensional CFD computation with four rotating blades could not be carried out during the design phase due to the high complexity and computation time effort. Unsteady two-dimensional calculations were carried out at six radial positions: $r/R = 0.39, 0.59, 0.70, 0.77, 0.86, 0.97$. At every radial position the local twist as well as the shifting of the rotation axis was considered. The estimate aerodynamic forces and moments were used for input of the finite element strength and fatigue calculations.

In order to determine the total loads and moments from the two dimensional calculations, the loads of the two dimensional sections were integrated spanwise. Due to the forward and backward swept planform the two dimensional calculations were carried out at six radial positions to get more supporting points for the integration. The forces and moments at the root and blade tip were assumed to be zero. From literature it is known that two dimensional dynamic stall CFD calculations tend to overestimate the aerodynamic forces and moments in comparison to three-dimensional computations [1]. Therefore the approach of the spanwise integration of two-dimensional forces and moments is a conservative assumption and ensure that the aerodynamic forces are not underestimated for the structural design.

For the unsteady two-dimensional CFD calculations the DLR-TAU code was used. All calculations were carried out fully turbulent with the Spalart-Allmaras turbulence model. The pitching periods were discretized with 1800 time steps per period and 600 inner iterations for every time step. The calculations are converged after five periods. A CFD mesh was built for both airfoils ($EDI-M112$ and $EDI-M109$). Four of the six used two-dimensional airfoil section meshes had to be adjusted in chord length and pitching axis due to tapering and sweep of the planform, see figure 5. Because the pitching point ($l/4$-line at the root) has to be shifted due to the spanwise sweep. The adjustments were done with the DLR-TAU setup tool. For the $EDI - M112$ airfoil a hybrid grid with 95,000 cells and a boundary layer discretization of 80 prisms was used. The grid of the $EDI - M109$ airfoil has 70,000 cells and a boundary layer discretization of 60 prisms.

For the design the aerodynamic forces and moments of a pitching cycle with $f_{rot} = 50Hz$ and $\alpha_{root}(t) = 10° + 8° \cdot sin(2\pi f_{rot} t)$ is calculated as a deep dynamic stall case. Additionally a static polar was calculated with the same rotation frequency to find the static stall angle. As in [1], it is assumed that the highest loads will occur at the deep dynamic stall case. For the centrifugal overload test a static polar at $f_{rot} = 65Hz$ was calculated to detect the collective angle with zero lift.

The integrated loads and pitching moment of the pitching cycle with $f_{rot} = 50Hz$ and $\alpha_{root}(t) = 10° + 8° \cdot sin(2\pi f_{rot} t)$ can be seen in figure 9. The blue dashed curve on the left graph represents the the lift trend at steady (collective) conditions. The static stall angle of attack is achieved at $\alpha_{s,s} = 10°$. After that the lift decreases smoothly. The blue continuous line is the lift curve of the pitching cycle. The typical lift overshoot can be seen. The lift increases up to an angle of attack of $\alpha = 16°$, then the lift declines strongly. At the same angle of attack a high decrease of the pitching moment can be observed on the right diagram. Both curves (unsteady lift and pitching moment) show a small short decrease before the increase to an unsteady stall angle of attack. This dent results from the beginning of the time shifting dynamic stall on the forward and backward swept part. The reattachment of the flow happens at $\alpha = 4.8°$. On the left diagram the drag is also depicted as continuous red line. The drag increases up to the unsteady angle of attack $\alpha = 16°$. Then the drag declines strongly. All trends show the typical hysteresis during the pitching cycle of the rotor blade.

These design load cases have been derived based on these results. The load cases used are the same as in [1]. Lc1 is the load case with the maximum flap bending. The second load case Lc2 considers the maximum rotor head shaft bending. The maximum pitching link load is covered by case Lc3. For this purpose the minimum pitching moment defines load case three Lc3. Load case four Lc4 is the maximum rotor thrust in combination with the maximum aerodynamic drag. The $f_{rot} = 65Hz$ overload case is load case five Lc5 with the maximum centrifugal forces at no rotor thrust. At load case six Lc6 the loss of one rotor blade is considered. For more information about the load cases see [1].

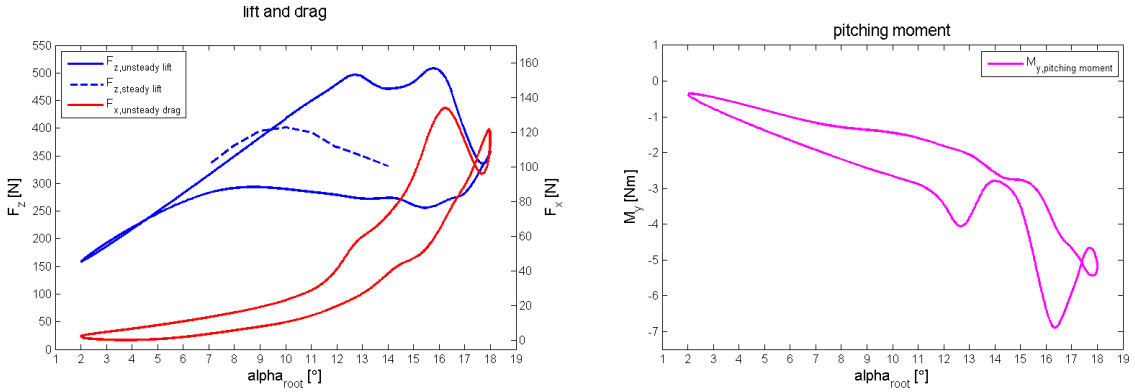

Fig. 9. Unsteady lift, drag and pitching moment for a pitching cycle $\alpha_{root}(t) = 10° + 8° \cdot sin(2\pi f_{rot} t)$ at $50Hz$

4.3 Structure design

The last step in the development was the structural design of the innovative double-swept rotor blade. The mechanical strength and fatigue behaviour had to be proven for all load cases. Therefore a safe operation of the model, on the Rotor Test Facility Goettingen can be ensured. The used FE model is depicted in figure 10. The FE model was assembled and based on the CAD geometry of the rotor blade. A finite element model of the rotor head already exists. It was created during the development of the RTG and the first set of rotor blades [1]. The full FE model for the calculations contains the new FE model of the innovative rotor blade connected to the rotor head. The rotor head FE model consists of the main shaft, all bearings, hulls and the blade connection. Only one blade was used in the full rotor head FE model to reduce the computational effort. The blade on the other side was replaced by its mass and resulting aerodynamic forces on the root. The commercial software ANSYS is used for the geometrical nonlinear FE analysis. The meshing tool is Altair Hypermesh. The FE model of the innovative double-swept rotor blade has 1661682 knots and 468751 elements.

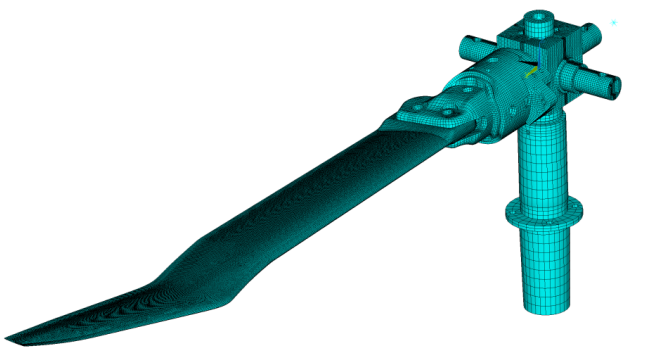

Fig. 10. Full finite element model of the innovative double-swept rotor blade with root adapter

The rotor blade is built from Carbon Fiber Reinforced Plastic (CFRP) with a foam core. The FE modeling of complex CFRP structures is a challenge due to the common orthotropic material properties (unidirectional layer). There are also carbon fiber laminates with isotropic material properties. A mix of carbon fiber laminate and unidirectional layer are necessary to exploit the advantages of CFRP over metal materials. The advantages of CFRP in comparison to metal materials are better mechanical strength properties at less weight. The FE model is build up of layers, the foam core and the resin. The inner volume consists of a foam core and a beam structure of UD-layers and laminates from two different carbon fibers depicted in figure 11. The outer upper and lower shells are modeled as a combination of UD-layers (unidirectional) and carbon fiber laminate. The UD-layers serve as a bending carrier. The planform is cut from a UD-laid. A high torsional stiffness is achieved through the fiber laminate layers. High shear stress areas in the forward and backward swept part occur due to the planform of the innovative rotor blade. Additional UD-layers of a second carbon fiber was added at high stress regions in the kink or the root.

The manufacturing of the rotor blades is done with two negative laminate forms. For the instrumentation the two half shells receive pocket millings for the pressure transducers. The carbon fibers in the inner volume of the rotor blade are damaged through the millings. Therefore the mechanical strength of the rotor blade is reduced. Due to the small dimension of the rotor blades, it is not possible to increase the number of UD-layers or carbon fiber laminates. These boundary conditions limit the achievable mechanical strength of the innovative rotor blades.

For the stress analysis all load cases were calculated. The loads were impressed on the FE model with the pressure distribution of the two dimensional sections. Between these two dimensional sections, the pressure distributions are interpolated linearly. At standard DLR stress analysis for wind tunnel models, safety factors of 2,5 and 4 are used. In this case a safety factor of 2 was

used for the innovative double-swept rotor blade. It is not possible to achieve a safety factor of 2,5 due to the complex planform, the instrumentation and dimension.

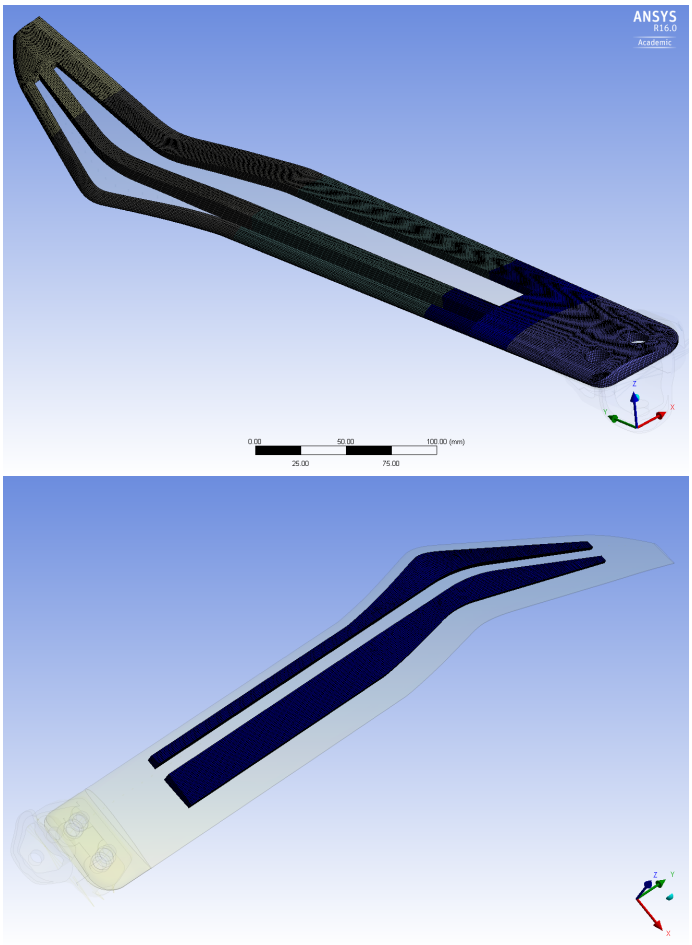

Fig. 11. Inner beam structure and foam core of the FE model

The rotor blade was investigated on two failure criterions: fiber fracture and intermediate fiber failure. For this the degree of utilization of the rotor blade is considered. The failure criterion is fulfilled if the degree of utilization is smaller than one. According to this criterion, the strength verification for the rotor blade is provided and the rotor blade is safe for operation. Multibody dynamic computations were performed to assess the stability of the new double-swept rotor blade at the RTG [12].

5 Conclusion

A new set of innovative double-swept rotor blades was developed at the DLR Goettingen in the Institut of Aeroelasticity. Investigations of dynamic stall and aeroelastic stability will be carried out with these rotor blades on the RTG Goettingen. The rotor test facility with the innovative rotor blades has a maximum radius of $R = 0.65$. The maximum operational rotation frequency is $f_{rot} = 50Hz$. Thereby Mach scaled measurements are possible. The achievable Reynolds number is ca. $Re = 1.0Mio$.
The development process included the complex CAD design, the unsteady CFD calculation, the derivation of the design loads from the CFD results, the definition of instrumentation and the FE analysis. The FE analysis included the structure modeling of FE model and the calculation of all load cases. In the future measurement campaigns will vary parameters like rotation frequency and angle of attack. The measurement techniques will be Stereo Pattern Recognition (deformation), blade tip camera, strain gauges (mode shape and deformation), pressure transducers (surface pressure), temperature sensors (surface temperature), piezoeletrical balance (forces and moments) and acceleration sensors (on the test rig).

Acknowledgment

Funding of the DLR project FAST Rescue is gratefully acknowledged. The author would like to thank T.Schwermer and H.Mai (DLR Goettingen) for all fruitful discussions and C.Stieg (DLR Goettingen) for his support in manufacturing.

References

[1] T. Schwermer, K. Richter and M. Raffel. Development of a rotor test facility for the investigation of dynamic stall. *New Results in Numerical and Experimental FluidMechanics X, Springer*, 6(7):663–673, 2016.

[2] T. Schwermer, A. Gardner and M. Raffel. Dynamic Stall Experiments on a Rotor with High Cyclic Setting in Axial Inflow. *Proceedings of the 73rd Annual Forum of the American Helicopter Societ, Milan*, 2017.

[3] J. Letzgus, T. Gardner, T. Schwermer, M. Kessler and E. Kraemer. Numerical Investigations of Dynamic Stall on a Rotor with Cyclic Pitch Control *Proceedings of the 43rd European Rotorcraft Forum, Milan*, 2017.

[4] A. Weiss, R. Geisler, T. Schwermer, D. Yorita, U. Henne, C. Klein and M. Raffel. Single-shot pressure-sensitive paint lifetime measurements on fast rotating blades using an optimized double-shutter technique. *Experiments in Fluids*, 58(9), 2017.

[5] B. Luetke, J. Nuhn, Y. Govers and M. Schmidt. design of a rotor blade tip for the investigation of dynamic stall in the transonic wind-tunnel Göttingen. *The aeronautical Journal*, 74(1232), 2016.

[6] B. Luetke. Dynamic Stall on a Pitching Double-Swept Rotor Blade Tip. *Technische Universität München*, 2017.

[7] B. Luetke, M. Schmidt, J. Sinske and J. Neumann. Structural design of an instrumented double-swept wind tunnel Model. *International Conference on Composite Materials, Copenhagen*, 2015.

[8] A. Goerttler, J. Braukmann, T. Schwermer, A. Gardner and M. Raffel. Tip-Vortex investigation on a rotating and pitching rotor blade. *43th European Rotorcraft Forum*, 2017.

[9] J. Braukmann, T. Schwermer and C. Wolf. Investigation of young blade-tip vortices at a rotor test facility using stereoscopic PIV. *Fachtagung "Experimentelle Stroemungsmechanik"*, 2017.

[10] W.R. Splettstoesser, J. Prieur, K. Pahlke, K.-J. Schultz, B.G. van der Wall, Y. Delrieux, P. Gardarein, P. Geoffroy and P. Leconte. Main Phase of the ERATO Cooperation on Aeroacoustic Rotor Optimization. *DLR Internal Report, DLR-IB 129-97/10*, Braunschweig, 1997.

[11] Y. Delrieux, J. Prieur, M. Costes, P. Gardarein, P. Beaumier, H.M. des Rochettes, P. Leconte, P. Crozier, W.R. Splettstoesser, B.G. van der Wall, B. Junker, K.-J. Schultz, E. Mercker, K. Pengel, J.J. Philippe and B. Gmelin. The ONERA-DLR Aeroacoustic Rotor Optimisation Programme ERATO: Methodology and Achievements. *American Helicopter Society Aerodynamics, Acoustics and Test and Evaluation Technical Specialists Meeting*, San Francisco, 2002.

[12] J. Arnold and S. Waitz. Using multibody dynamics for the stability assessment of a new double-swept rotor blade setup. *44th European Rotorcraft Forum*, Delft, 2018.